

Collapse and Fragmentation of Molecular Cloud Cores. IX. Magnetic Braking of Initially Filamentary Clouds.

Alan P. Boss

*Department of Terrestrial Magnetism, Carnegie Institution of Washington, 5241 Broad
Branch Road, NW, Washington, DC 20015-1305*

boss@dtm.ciw.edu

ABSTRACT

The collapse and fragmentation of initially filamentary, magnetic molecular clouds is calculated in three dimensions with a gravitational, radiative hydrodynamics code. The code includes magnetic field effects in an approximate manner: magnetic pressure, tension, braking, and ambipolar diffusion are all modelled. The parameters varied are the ratio of the ambipolar diffusion time to the free fall time at the center of the filamentary cloud ($t_{ad}/t_{ff} = 10, 20, \text{ or } 10^6 \sim \infty$), the cloud's reference magnetic field strength ($B_{oi} = 0, 200, \text{ or } 300$ microgauss – the latter two values leading to magnetically subcritical clouds), the ratio of rotational to gravitational energy of the filament (10^{-4} or 10^{-2}), and the efficiency of magnetic braking (represented by a factor $f_{mb} = 0, 10^{-4}, \text{ or } 10^{-3}$). Three types of outcomes are observed: direct collapse and fragmentation into a multiple protostar system (models with $B_{oi} = 0$), periodic contraction and expansion without collapse (models with $t_{ad}/t_{ff} = 10^6$), or periodic contraction and expansion leading eventually to collapse on a time scale of ~ 6 to $12 t_{ff}$ (all other models). Because the computational grid is a finite volume sphere, the expanding clouds bounce off the spherical boundary and re-collapse toward the center of the spherical grid, leading to the periodic formation of shocked regions where the infalling gas collides with itself, forming dense layers susceptible to sustained collapse and eventual fragmentation. While the models begin their evolution at rest except for the assumed solid-body rotation, they develop weakly supersonic velocity fields as a result of the rebounding prior to collapse. The models show that magnetically-supported clouds subject to magnetic braking can undergo dynamic collapse leading to protostellar fragmentation on scales of 10 AU to 100 AU, consistent with typical binary star separations.

Subject headings: hydrodynamics — ISM: clouds — ISM: kinematics and dynamics — MHD — stars: formation

1. Introduction

Theoretical interest in the effects of magnetic fields on the star formation process continues to be strong (e.g., Krasnopolsky & Gammie 2005; Machida et al. 2006; Galli et al. 2006; Shu et al. 2006) in spite of the ongoing debate concerning the relative importance of turbulence and magnetic fields for cloud support (e.g., Nakamura & Li 2005). Mouschovias, Tassis, & Kunz (2006) have argued that existing measurements of magnetic field strengths in molecular clouds are in quantitative agreement with the predictions of star formation theories where molecular clouds are supported against gravitational collapse primarily by magnetic fields, with this magnetic support being gradually lost as a result of ambipolar diffusion of the magnetic fields.

There is strong observational evidence that magnetic fields are important for the support of pre-collapse molecular clouds and cores (e.g., Crutcher 1999). Recently, observations have revealed a low-mass binary protostellar system (NGC 1333 IRAS 4A) where polarized dust emission implies a magnetic field geometry that is consistent with theoretical expectations for the collapse of a magnetized, molecular cloud: an hourglass shape for the magnetic field, with a field strength that dominates turbulent motions (Girat, Rao, & Marrone 2006). While turbulence may dominate in some star-forming regions, clearly there are other regions where magnetic fields are dominant.

The present series of papers (i.e., Boss 1997, 1999, 2002, 2005 – magnetic fields were not included in the first four papers in the series) has attempted to determine the conditions under which a magnetically-supported cloud core can collapse and fragment into a binary or multiple protostellar system, as a result of gravitational collapse initiated by ambipolar diffusion. These three-dimensional radiative hydrodynamical models have included a crude representation of magnetic field effects, based on several approximations for the magnetohydrodynamical (MHD) equations. However, certain effects, such as magnetic field flattening of collapsing clouds and magnetic braking of cloud rotation, have not been included in the models. Here we address the latter concern, by including a new approximation for magnetic braking.

Magnetic braking can be quite effective at reducing cloud rotation rates during the pre-collapse cloud phase (Basu & Mouschovias 1994, 1995a,b), but the progressive loss of magnetic flux by ambipolar diffusion eventually greatly weakens this effect and once the magnetic field has been reduced sufficiently, the cloud begins to collapse. Basu & Mouschovias (1994, 1995a,b) found as a result that magnetic braking had little effect during the collapse phase, with the cloud core’s angular momentum being approximately conserved during collapse. However, Hosking & Whitworth (2004) concluded that rotationally-driven fragmentation could be halted by magnetic braking, though the thermodynamical treatment

employed could also have been responsible at least in part for their results (Boss 2004).

In this paper we develop an approximation for magnetic braking, based on the more detailed models of Basu & Mouschovias (1994), and apply this approximation to the three-dimensional collapse and fragmentation of initially filamentary, magnetic clouds. Observations of star formation in the Perseus molecular cloud point to filamentary structures on both large and small scales, with the filaments being dense enough to be gravitationally unstable (Hatchell et al. 2005). Filamentary geometries are also attractive theoretically for cloud fragmentation studies (Larson 2005).

2. Numerical Methods

The numerical models are calculated with a three-dimensional hydrodynamics code that calculates finite-difference solutions of the equations of radiative transfer, hydrodynamics, and gravitation for a compressible fluid (Boss & Myhill 1992). The hydrodynamic equations are solved in conservation law form on a contracting spherical coordinate grid, subject to constant volume boundary conditions on the spherical boundary. The code is second-order-accurate in both space and time, with the van Leer-type hydrodynamical fluxes having been modified to improve stability (Boss 1997). Artificial viscosity is not employed. Radiative transfer is handled in the Eddington approximation, including detailed equations of state and dust grain opacities (e.g., Pollack et al. 1994). The code has been tested on a variety of test problems (Boss & Myhill 1992; Myhill & Boss 1993).

The Poisson equation for the cloud’s gravitational potential is solved by a spherical harmonic expansion (Y_{lm}) including terms up to $N_{lm} = 32$. The computational grid consists of a spherical coordinate grid with $N_r = 200$, $N_\theta = 22$ for $\pi/2 \geq \theta \geq 0$ (symmetry through the midplane is assumed for $\pi \geq \theta > \pi/2$), and $N_\phi = 256$ for $2\pi \geq \phi \geq 0$, i.e., with no symmetry assumed in ϕ . The radial grid contracts to follow the collapsing inner regions and to provide sufficient spatial resolution to ensure satisfaction of the four Jeans conditions for a spherical coordinate grid (Truelove et al. 1997; Boss et al. 2000). The innermost 50 radial grid points are kept uniformly spaced during grid contraction, while the outermost 150 are non-uniformly spaced, in order to provide an inner region with uniform spatial resolution in the radial coordinate. The ϕ grid is uniformly spaced, whereas the θ grid is compressed toward the midplane, where the minimum grid spacing is 0.3 degrees.

3. Magnetic Field Approximations

As in the previous three-dimensional models (Boss 1997, 1999, 2002, 2005), the effects of magnetic fields are approximated through the use of several simplifying approximations, which are briefly reviewed here.

3.1. Previous Approximations

The effective magnetic pressure ($B^2/8\pi$) is added in with the gas pressure (p), an approximation that is exact for high conductivities and straight field lines. Even with low fractional ionizations, molecular clouds have extremely high conductivities. Furthermore, calculations of the axisymmetric contraction of magnetic clouds show that initially straight magnetic field lines remain remarkably straight throughout the ambipolar diffusion phase, and only begin bending significantly once dynamic collapse begins near the center of the cloud (e.g., Fiedler & Mouschovias 1993). For the present models of initially filamentary clouds, the magnetic field is assumed to be initially straight and aligned with the major axis of the filaments, preserving the accuracy of this approximation. However, because the models assume that B depends on the gas density (see below), as the filamentary clouds evolve and become highly non-filamentary (see Figures in the Results section), evidently this approximation becomes increasingly less appropriate. This fact, as well as the other approximations employed in these pseudo-MHD calculations, emphasizes the need for the predictions of these models to be rechecked with a true MHD code.

Once collapse proceeds to a significant extent, magnetic field lines will bend and exert a tension force that counteracts gravity. For a thin disk with a constant mass-to-flux ratio, the magnetic tension is proportional to the gravitational acceleration (Basu 1997; Shu & Li 1997; Nakamura & Hanawa 1997). Note that while this approximation is exact for a thin disk, the present models are intended to represent three dimensional filaments, and so the magnetic tension approximation will not be exact and will need to be reinvestigated with a future true MHD code. The magnetic tension in the thin disk approximation can be included (Boss 2000) simply by modifying the gravitational potential Φ as follows

$$\nabla\Phi \rightarrow \left(1 - \frac{1}{2} \frac{\nabla \frac{B^2}{8\pi}}{\nabla p}\right) \nabla\Phi.$$

This magnetic tension approximation is only employed in the present models once the clouds have collapsed enough to begin to form rotationally flattened disks, i.e., after densities above $\sim 10^{-15} \text{ g cm}^{-3}$ are reached at the center of the cloud. Fragmentation only occurs after

much higher densities are reached ($\sim 10^{-11}$ g cm $^{-3}$). Boss (2002) computed five collapse models (P2A, P2B, P2C, P2D, P2E) identical to five models (l, ab, z, s, m) in Boss (1999) except for having used the magnetic tension approximation, finding that the magnetic tension approximation led to fragmentation even in slowly rotating clouds that did not fragment in the absence of this approximation.

For an isothermal gas and a magnetic field B that varies with density ρ as $B \propto \rho^\kappa$, with $\kappa = 1/2$ (as is found in detailed MHD calculations, e.g., Ciolek & Mouschovias 1995), magnetic tension forces can be approximated by diluting the gravitational potential by a factor involving a function only of time

$$\Phi \rightarrow \Phi \times (1 - \frac{1}{2}f(t)),$$

where $f(t)$ is a factor of order unity that decreases with time due to the effects of ambipolar diffusion.

3.2. Magnetic Braking Approximation

The random orientations of T Tauri star outflow axes with respect to the local magnetic field directions suggests that magnetic fields do not determine the final rotation axes of protostars (Ménard & Duchêne 2004). Nevertheless, it is important to consider the effects of magnetic braking during cloud collapse and fragmentation, in order to constrain the effectiveness of magnetic fields in transporting angular momentum. A new approximation is derived here for magnetic braking.

We consider the case of clouds where the initial angular velocity is aligned with the initial magnetic field direction, i.e., with both aligned along the \hat{z} axis. Magnetic braking of the ϕ component of the velocity then derives from the following magnetic force term:

$$\rho \frac{\partial v_\phi}{\partial t} + \rho \vec{v} \cdot \nabla v_\phi = \dots + \frac{1}{4\pi} (\vec{B} \cdot \nabla) B_\phi.$$

Initially $B_\phi = 0$ and $B_R = 0$, and throughout most of the collapse phase $|B_\phi| \ll B_z$ and $B_R < B_z$ (Basu & Mouschovias 1994), so that $B_z \approx B$, the total magnetic field (note that R and z are cylindrical coordinates). From Figure 7 of Basu & Mouschovias (1994), $|B_\phi| \approx 10^{-4} B_z$ once contraction begins. Magnetic braking can then be approximated by including the following magnetic force term:

$$\rho \frac{\partial v_\phi}{\partial t} + \rho \vec{v} \cdot \nabla v_\phi = \dots + f_{mb} \left(\frac{\partial}{\partial R} + \frac{\partial}{\partial z} \right) \left(\frac{B^2}{8\pi} \right),$$

where $f_{mb} \sim 10^{-4}$ is a parameter that controls the strength of the magnetic braking. Given the magnitude of f_{mb} , magnetic braking is expected to be a relatively small effect, as was found by Basu & Mouschovias (1994) in their two-dimensional calculations. In the spherical coordinate system used in the present code, this approximation becomes

$$\rho \frac{\partial v_\phi}{\partial t} + \rho \vec{v} \cdot \nabla v_\phi = \dots + f_{mb} \left(\frac{\partial}{\partial r} - \frac{1}{r} \frac{\partial}{\partial \theta} \right) \left(\frac{B^2}{8\pi} \right).$$

Note that the contributions from both the r and θ derivatives are defined to be negative (given that B generally increases toward the cloud center and toward the cloud midplane) and so will result in a loss of the total angular momentum of the cloud, i.e., the losses due to magnetic braking are maximized in this approximation.

The gravitational potential Φ dilution approximation ultimately derives from the same magnetic tension term from which the magnetic braking approximation is derived, but it was derived in the context of axisymmetric magnetic disks and so was not intended to represent magnetic braking through ϕ gradients of Φ . While ϕ gradients of Φ could lead to forces in the ϕ direction that could be identified with magnetic braking (or acceleration) in the thin disk approximation, in practice these gradients lead primarily to local, not to global losses of the total angular momentum of the cloud. In fact, most of the total angular momentum loss occurs early in the evolution of these models, well before the Φ dilution approximation is initiated. Very little loss of the total angular momentum of the cloud occurs after that point. Global angular momentum loss however is what is desired, in order to mimic the magnetic braking caused by magnetic field lines that thread the cloud and transport angular momentum out of the cloud to an external medium. As there is no external medium in the present calculations, the magnetic braking approximation derived above is meant to represent losses to such a medium and should result in global loss of the total cloud angular momentum. This loss of total angular momentum occurs in the models, as mentioned in the *Results* section. Because the magnetic pressure is added directly in with the gas pressure, the ϕ gradients of the total pressure (gas plus magnetic field) are also source terms for the specific angular momentum equation, and so can act to transport angular momentum locally.

4. Initial Conditions

Tables 1, 2, and 3 list the initial conditions for the models. The variations explored include the ambipolar diffusion time scale ($t_{ad} = 10, 20$, or $10^6 t_{ff}$, where $t_{ff} = (3\pi/32G\rho_0)^{1/2} = 3.3 \times 10^4$ yr), the magnetic braking factor ($f_{mb} = 0.0, 0.0001$, or 0.001), the reference magnetic field strength ($B_{oi} = 0, 200$, or $300 \mu\text{G}$), and the angular velocity about an axis perpendicular to the long axis of the filament ($\Omega_i = 10^{-14}$ or 10^{-13} rad s $^{-1}$). These choices of Ω_i result in initial ratios of rotational to gravitational energy of $\beta_i = 0.0001$ and 0.01 , respectively. Clouds with $B_{oi} = 200$ or $300 \mu\text{G}$ have initial ratios of magnetic to gravitational energy of $\gamma_i = 0.26$ or 0.59 . The mass to flux ratio of these clouds is less than the critical mass to flux ratio, making both clouds formally magnetostatically stable and hence magnetically subcritical.

The initial filamentary geometries are specified by starting with prolate spheroids with 40 to 1 axis ratios between the one long and two short axes. The filaments initially have a Gaussian radial density profile as in Boss (1997), with $r_a = 11.6R$ and $r_b = r_c = 0.29R$ (R is the cloud radius) and with a maximum density $\rho_0 = 4.0 \times 10^{-18}$ g cm $^{-3}$. An initial density perturbation consisting of 50% noise is applied to each computational cell. The cloud radius is $R = 1.0 \times 10^{17}$ cm ≈ 0.032 pc for all models. Each cloud has a total mass of $1.27 M_\odot$ and begins with an initial ratio of thermal to gravitational energy of $\alpha_i = 0.35$.

5. Results

Tables 1, 2, and 3 list the initial conditions as well as the basic outcome of each model, namely the final time to which the cloud was advanced t_f (in units of the initial cloud free fall time) and whether the cloud eventually underwent sustained collapse (C) leading to protostar formation.

5.1. Non-Magnetic Collapse

Figure 1 shows the initial filamentary cloud used for all of the models, both magnetic and non-magnetic. The filament is initially oriented along the \hat{x} axis, rotating counter-clockwise about the \hat{z} axis, perpendicular to the equatorial plane shown. The initial Gaussian radial density distribution falls off rapidly with distance away from the \hat{x} axis, reaching a value at the cloud boundary $\sim 10^5$ smaller than the initial density in the filament.

Figure 2 shows that after $1.429 t_{ff} \approx 4.7 \times 10^4$ yr, the filament has contracted inward

along its length and begun to fragment into three protostellar clumps, one at the center of the filament, and one at each end. Model mbfb evolves in the same manner as model mbfa, the only difference being that the filament rotates through an angle of $\sim 10^\circ$ by the same phase of evolution due to its higher initial angular velocity. Because of the nature of the spherical coordinate grid used in these models, where the grid is designed to be refined as needed for collapse at the center of the spherical volume, it is not possible to calculate the further evolution of models mbfa (or mbfb) beyond the phase shown in Figure 2 without violating the Jeans criterion for maintaining sufficient spatial resolution to avoid spurious fragmentation. However, given that the filament has clearly fragmented into at least two well-defined clumps while satisfying the Jeans criterion, it is likely that the two filament-end clumps would continue to grow and survive the subsequent close encounters with each other near the center of the cloud, and thus form a binary (if not higher order) protostellar system. Similar models of the fragmentation of elongated cylindrical clouds demonstrating this outcome were performed by Bastien et al. (1991).

5.2. Magnetic Collapse

Models mbfa and mbfb demonstrated that in the absence of magnetic fields, these filamentary clouds would promptly contract and fragment into binary or multiple protostar systems, on a free fall time scale. We now turn to the magnetic cloud models, to learn what happens to magnetically subcritical clouds subject to ambipolar diffusion.

Figures 3 through 8 depict the evolution of model mbf2g, in which no magnetic braking was assumed ($f_{mb} = 0$). Comparing Figures 2 and 3, it is clear that when magnetic fields are included, the magnetic cloud contracts inward along the axis of the filament, but does not contract significantly along its minor axes, compared to the non-magnetic cloud mbfa, and shows no tendency to fragment on the free fall time scale. Rather, the two ends of the filament collide at the cloud center (Figure 4), forming an oblate cloud with the major axis of the pancake perpendicular to the equatorial plane. Meanwhile, gas which had been forced away from the initial filament (along the \hat{y} axis) rebounds off the outer cloud boundary and begins to fall back toward the center, as the central oblate portion reexpands (Figure 5). The infalling gas forms two well-defined shock fronts (Figure 6), which meet at the center to produce a high density cloud that is more prolate than oblate (Figure 7). At this point the cloud begins a sustained self-gravitational collapse, and fragments into a binary protostellar system (Figure 8), composed of two marginally gravitationally bound clumps with masses of $\sim 10^{-3}M_\odot$ and maximum temperatures ~ 20 K.

By way of comparison, Figure 9 shows the outcome of model mbf2e, where magnetic

braking was applied at the maximum level considered to be appropriate ($f_{mb} = 0.001$), based on the models of Basu & Mouschovias (1994). Figure 9 shows that even with loss of angular momentum by magnetic braking, these filamentary clouds are still able to collapse and fragment into binary systems. This is because in these models, the fragmentation that occurs is not rotationally driven, i.e., it is not a result of starting the clouds with relatively high initial rotation rates, such as $\beta_i \sim 0.1$, but with $\beta_i = 0.01$ or 0.0001 . By comparison, the models of Hosking & Whitworth (2004) started with $\beta_i \sim 0.05$ and needed rapid rotation to fragment. In fact, the choice of β_i has little direct effect on the outcome of the present models: models mbf2c, mbf2e, and mbf2g all started with $\beta_i = 0.0001$ and formed binary systems, whereas models mbf2d, mbf2f, and mbf2h with $\beta_i = 0.01$ appeared to collapse to form single protostars. Figure 10 shows the outcome of model mbf2f for comparison with mbf2e – a single protostar forms, with a maximum density of $4 \times 10^{-10} \text{ g cm}^{-3}$ and a maximum temperature of 79 K.

While magnetic braking thus had little effect on the outcomes with respect to fragmentation into binary protostars, it did have an appreciable effect on the evolution of the total angular momentum of the clouds. With $f_{mb} = 0.001$, the clouds typically lost $\sim 10 \%$ of their total angular momentum during the evolutions, whereas with $f_{mb} = 0.0001$, the losses were at most a few percent. For the non-magnetic clouds, the total angular momentum was conserved throughout the evolution, consistent with the solution of the momentum equations in conservation law form.

The models with higher initial magnetic field strength (Table 3) evolved qualitatively in the same manner as the less magnetically subcritical models (Table 2) discussed so far. The main difference was that their evolutions required longer time periods before dynamic collapse was achieved, even for the same values of the ambipolar diffusion time scales. Figure 11 shows the result of model mbfn, where the cloud fragments into four distinct clumps after $12.091 t_{ff}$. With $f_{mb} = 0.0001$, model mbfj fragmented into only two clumps, showing that in these two cases, magnetic braking may have been able to reduce somewhat the extent of fragmentation during the collapse phase.

In the models with essentially infinite ambipolar diffusion time scales, the clouds periodically contracted and rebounded for times as long as $\sim 25 t_{ff}$ without ever achieving dynamic collapse, as expected. The total magnetic energy in these models with effectively frozen-in fields is conserved to $\sim 0.1\%$ during these lengthy evolutions, whereas the total magnetic energy drops to ~ 0.1 its initial value in the models with significant ambipolar diffusion.

6. Discussion

Magnetic braking was not terribly effective in these models, even in the models with $f_{mb} = 0.001$, a factor of ten times higher than estimated on the basis of the work of Basu & Mouschovias (1994). This inefficiency is attributed in part to the relatively slow initial cloud rotation rates assumed, and hence the lack of rotationally-driven fragmentation even in the models without magnetic braking.

While the models begin with filamentary cloud geometries, the strong degree of initial magnetic support does not allow them to undergo dynamic collapse following their initial contraction inwards along the length of the filaments. Instead, the contracting filaments rebound outward. Meanwhile, the portions of the initial cloud that had expanded outward in the directions perpendicular to the long axis of the filament are bounced back toward the center of the cloud after striking the outer boundary. These two portions then fall back toward each other, meeting and merging at the center to form a new highly prolate, dense cloud, which may then be able to begin sustained dynamic collapse as a result of ambipolar diffusion, or which may begin another cycle of outward rebounding followed by inward collapse.

In model mbf2n, e.g., large-scale shock-like structures traverse the cloud radius of 0.032 pc in about $2 t_{ff}$, implying mean speeds of $\sim 0.3 \text{ km s}^{-1}$, slightly above the sound speed of 10 K gas of 0.2 km s^{-1} . Hence these clouds develop transient bursts of weakly supersonic motions across length scales of order 0.064 pc (the cloud diameter). While both inward and outward motions occur at similar speeds, the dominant motions of dense gas tend to be inward, as the rebounding clouds falls back toward its center of gravity.

The rebounding of the clouds off the outer boundary of the calculational volume is an artificial effect, though one could imagine that if a series of adjacent filaments were undergoing collapse, their interactions might lead to expanding regions that impact each other in much the same way as occurs in these models. From this point of view, the fixed volume boundary conditions can be viewed as a crude form of periodic boundary conditions, representing a molecular cloud complex filled with spherical segments of continuous filaments. The rebounding filaments then impact each other in a somewhat chaotic manner until such time as a self-gravitating cloud core forms and begins to undergo dynamic gravitational collapse. These unstable cloud cores form where the velocity flows converge at mildly supersonic speeds.

7. Conclusions

From Figures 8, 9, and 11, we see evidence for protostellar fragmentation into binary or multiple systems with separations on the order of 10 AU to 100 AU. The models thus show that magnetically-supported clouds subject to magnetic braking can undergo dynamic collapse leading to protostellar fragmentation on scales of order 30 AU, roughly consistent with the mean of the distribution of observed binary star separations. While Hosking & Whitworth (2004) showed how magnetic braking might suppress the fragmentation of initially rapidly rotating clouds, the present models show that when radiative transfer is coupled with a crude treatment of magnetic braking, relatively slowly rotating, magnetic clouds can still collapse and fragment in some cases into binary protostellar systems with appropriate initial separations.

While somewhat artificial boundary conditions have been employed, the models also show how the resulting regions of converging velocity fields in magnetic, molecular clouds can lead to the transient formation of dense, highly prolate cloud cores, which may or may not be able to immediately undergo collapse to form protostellar systems. In comparison to purely hydrodynamical models where an initially turbulent, supersonic velocity field is assumed (e.g., Klessen, Heitsch, & Mac Low 2000), the present magnetic cloud models show how even in the case of an initially static (except for solid-body rotation) filamentary cloud, the evolution of the cloud is to undergo a series of asymmetric contractions and rebounds that can lead to the generation of weakly supersonic velocity fields across the length scale of the initial clouds (i.e., ~ 0.1 pc in the present models). Sustained dynamic collapse then only occurs on the ambipolar diffusion time scale, rather than on the free fall time of the cloud.

Supersonic turbulent velocity fields capable of supporting molecular clouds against collapse tend to dissipate through shock formation on time scales of the cloud free fall time, unless some source capable of continually driving the turbulence is postulated, e.g., stellar outflows. Magnetic fields strong enough for magnetostatic support (i.e., magnetically subcritical clouds) can prevent cloud collapse on the cloud free fall time scale (e.g., Ostriker, Gammie, & Stone 1999; Heitsch, Mac Low, & Klessen 2001). The question of cloud support by supersonic turbulence, magnetic fields, or some combination of the two is critical for understanding star formation rates and lifetimes of molecular cloud complexes (Mouschovias et al. 2006). The present models suggest that even in the case of initially magnetostatic clouds, ambipolar diffusion can lead to the generation of weakly supersonic, large-scale motions, eventually leading to sustained dynamic collapse and protostellar fragmentation, on a time scale determined primarily by that for ambipolar diffusion. However, given the crudeness of the MHD approximations employed in these and in the previous models, these

suggestions must be considered provisional, subject to revision by calculations that include a true solution of the magnetic induction equation.

The numerical calculations were performed on the Carnegie Alpha Cluster, which, along with this work, is partially supported by the National Science Foundation under grants AST-0305913 and MRI-9976645. I thank Sandy Keiser for cluster and workstation system management and the referee for a number of helpful comments about the manuscript.

REFERENCES

- Bastien, P., Arcoragi, J.-P., Benz, W., Bonnell, I., & Martel, H. 1991, *ApJ*, 378, 255
- Basu, S. 1997, *ApJ*, 485, 240
- Basu, S., & Mouschovias, T. Ch. 1994, *ApJ*, 432, 720
- . 1995a, *ApJ*, 452, 386
- . 1995b, *ApJ*, 453, 271
- Boss, A. P. 1997, *ApJ*, 483, 309
- . 1999, *ApJ*, 520, 744
- . 2000, *ApJ*, 545, L61
- . 2002, *ApJ*, 568, 743
- . 2004, *MNRAS*, 350, L57
- . 2005, *ApJ*, 622, 393
- Boss, A. P., Fisher, R. T., Klein, R. I., & McKee, C. F. 2000, *ApJ*, 528, 325
- Boss, A. P., & Myhill, E. A. 1992, *ApJS*, 83, 311
- Ciolek, G. E., & Mouschovias, T. Ch. 1995, *ApJ*, 454, 194
- Crutcher, R. M. 1999, *ApJ*, 520, 706
- Fiedler, R. A., & Mouschovias, T. Ch. 1993, *ApJ*, 415, 680
- Galli, D., Lizano, S., Shu, F. H. & Allen, A. 2006, *ApJ*, 647, 374
- Girat, J. M., Rao, R. & Marrone, D. P. 2006, *Science*, 313, 812
- Hatchell, J., et al. 2005, *A&A*, 440, 151
- Heitsch, F., Mac Low, M.-M., & Klessen, R. S. 2001, *ApJ*, 547, 280
- Hosking, J. G., & Whitworth, A. P. 2004, *MNRAS*, 347, 1001

- Klessen, R. S., Heitsch, F., & Mac Low, M.-M. 2000, *ApJ*, 535, 887
- Krasnopolsky, R. & Gammie, C. F. 2005, *ApJ*, 635, 1126
- Larson, R. B. 2005, *MNRAS*, 359, 211
- Machida, M. N., Matsumoto, T., Hanawa, T. & Tomisaka, K. 2006, *ApJ*, 645, 1227
- Ménard, F., Duchêne, G. 2004, *A&A*, 425, 973
- Mouschovias, T. Ch., Tassis, K. & Kunz, M. W. 2006, *ApJ*, 646, 1043
- Myhill, E. A., & Boss, A. P. 1993, *ApJS*, 89, 345
- Nakamura, F., & Hanawa, T. 1997, *ApJ*, 480, 701
- Nakamura, F. & Li, Z.-Y. 2005, *ApJ*, 631, 411
- Ostriker, E., Gammie, C. F., & Stone, J. M. 1999, *ApJ*, 513, 259
- Pollack, J. B., Hollenbach, D., Beckwith, S., Simonelli, D. P., Roush, T., & Fong, W. 1994, *ApJ*, 421, 615
- Shu, F. H., Galli, D., Lizano, S. & Cai, M. 2006, *ApJ*, 647, 382
- Shu, F. H., & Li, Z.-Y. 1997, *ApJ*, 475, 251
- Truelove, J. K., Klein, R. I., McKee, C. F., Holliman, J. H., Howell, L. H., & Greenough, J. A. 1997, *ApJ*, 489, L179

Table 1. Initial conditions and results for two non-magnetic, filamentary clouds. In this table and the following, ambipolar diffusion times t_{ad} and final times t_f are given in units of the initial free fall time $t_{ff} = (3\pi/32G\rho_0)^{1/2} = 3.3 \times 10^4$ yr. The magnetic braking factor f_{mb} is dimensionless, while the units for Ω_i are rad s^{-1} . C denotes a cloud that collapses, while R denotes a cloud that rebounds indefinitely without collapsing.

model	t_{ad}/t_{ff}	f_{mb}	Ω_i	t_f/t_{ff}	result
mbfa	0	0.0	10^{-14}	1.43	C
mbfb	0	0.0	10^{-13}	1.46	C

Table 2. Initial conditions and results for filamentary clouds with magnetic braking and $B_{oi} = 200$ microgauss, as in Table 1.

model	t_{ad}/t_{ff}	f_{mb}	Ω_i	t_f/t_{ff}	result
mbf2c	10	0.0001	10^{-14}	5.699	C
mbf2d	10	0.0001	10^{-13}	6.056	C
mbf2e	10	0.001	10^{-14}	5.707	C
mbf2f	10	0.001	10^{-13}	6.056	C
mbf2g	10	0.0	10^{-14}	5.698	C
mbf2h	10	0.0	10^{-13}	6.061	C
mbf2i	20	0.0001	10^{-14}	7.667	C
mbf2j	20	0.0001	10^{-13}	8.158	C
mbf2k	20	0.001	10^{-14}	7.726	C
mbf2l	20	0.001	10^{-13}	8.126	C
mbf2m	20	0.0	10^{-14}	7.669	C
mbf2n	20	0.0	10^{-13}	8.136	C

Table 3. Initial conditions and results for filamentary clouds with magnetic braking and $B_{oi} = 300$ microgauss, as in Table 1.

model	t_{ad}/t_{ff}	f_{mb}	Ω_i	t_f/t_{ff}	result
mbfc	10	0.0001	10^{-14}	6.06	C
mbfd	10	0.0001	10^{-13}	6.33	C
mbfe	10	0.001	10^{-14}	6.03	C
mbff	10	0.001	10^{-13}	6.31	C
mbfg	10	0.0	10^{-14}	6.05	C
mbfh	10	0.0	10^{-13}	6.31	C
mbfi	20	0.0001	10^{-14}	11.67	C
mbfj	20	0.0001	10^{-13}	12.07	C
mbfk	20	0.001	10^{-14}	11.67	C
mbfl	20	0.001	10^{-13}	12.09	C
mbfm	20	0.0	10^{-14}	11.76	C
mbfn	20	0.0	10^{-13}	12.09	C
mbfo	10^6	0.0001	10^{-14}	25.2	R
mbfp	10^6	0.0001	10^{-13}	24.6	R
mbfq	10^6	0.001	10^{-14}	11.83	R
mbfr	10^6	0.001	10^{-13}	7.96	R
mbfs	10^6	0.0	10^{-14}	6.46	R
mbft	10^6	0.0	10^{-13}	16.2	R

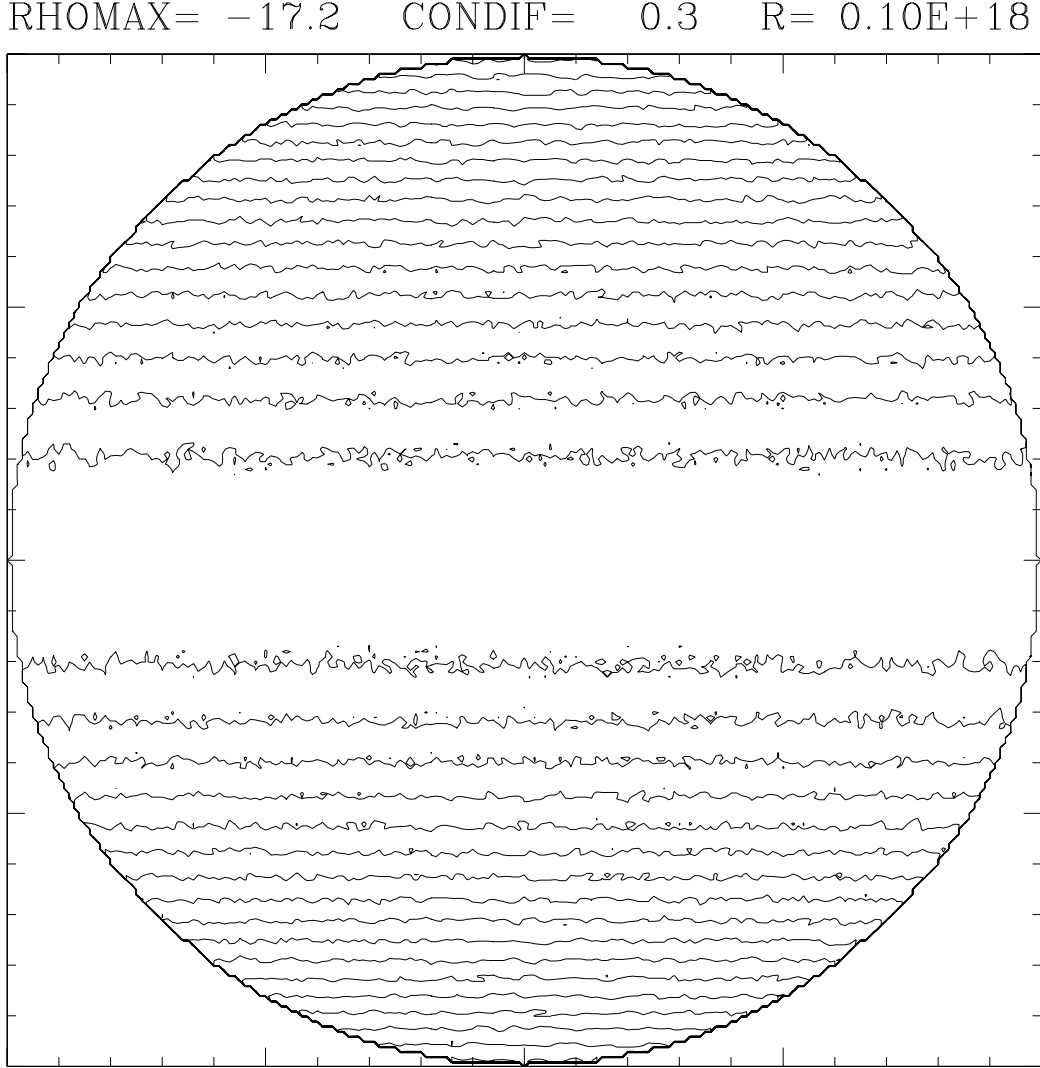


Fig. 1.— Initial density contours in the equatorial plane for model mbfa, and for all the other models as well. Maximum density is $6.3 \times 10^{-18} \text{ g cm}^{-3}$. Contours represent changes by a factor of 2 in density. Region shown is $1.0 \times 10^{17} \text{ cm}$ in radius. The filamentary cloud is oriented horizontally initially.

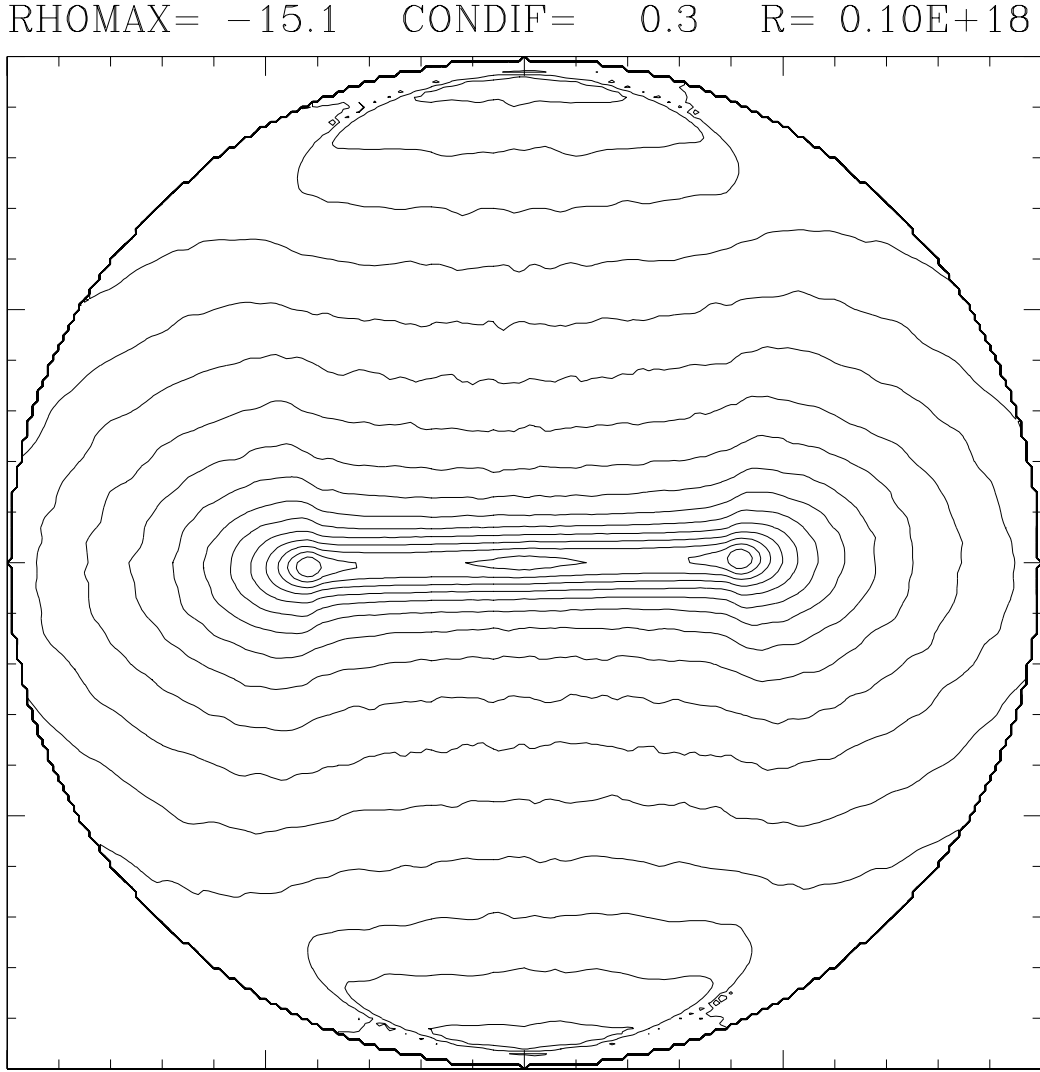


Fig. 2.— Density contours in the equatorial plane for non-magnetic model mbfa after $1.429 t_{ff}$, plotted as in Figure 1. Maximum density is $7.9 \times 10^{-16} \text{ g cm}^{-3}$. The filamentary cloud has collapsed inward along its length and begun to fragment into three protostellar clumps.

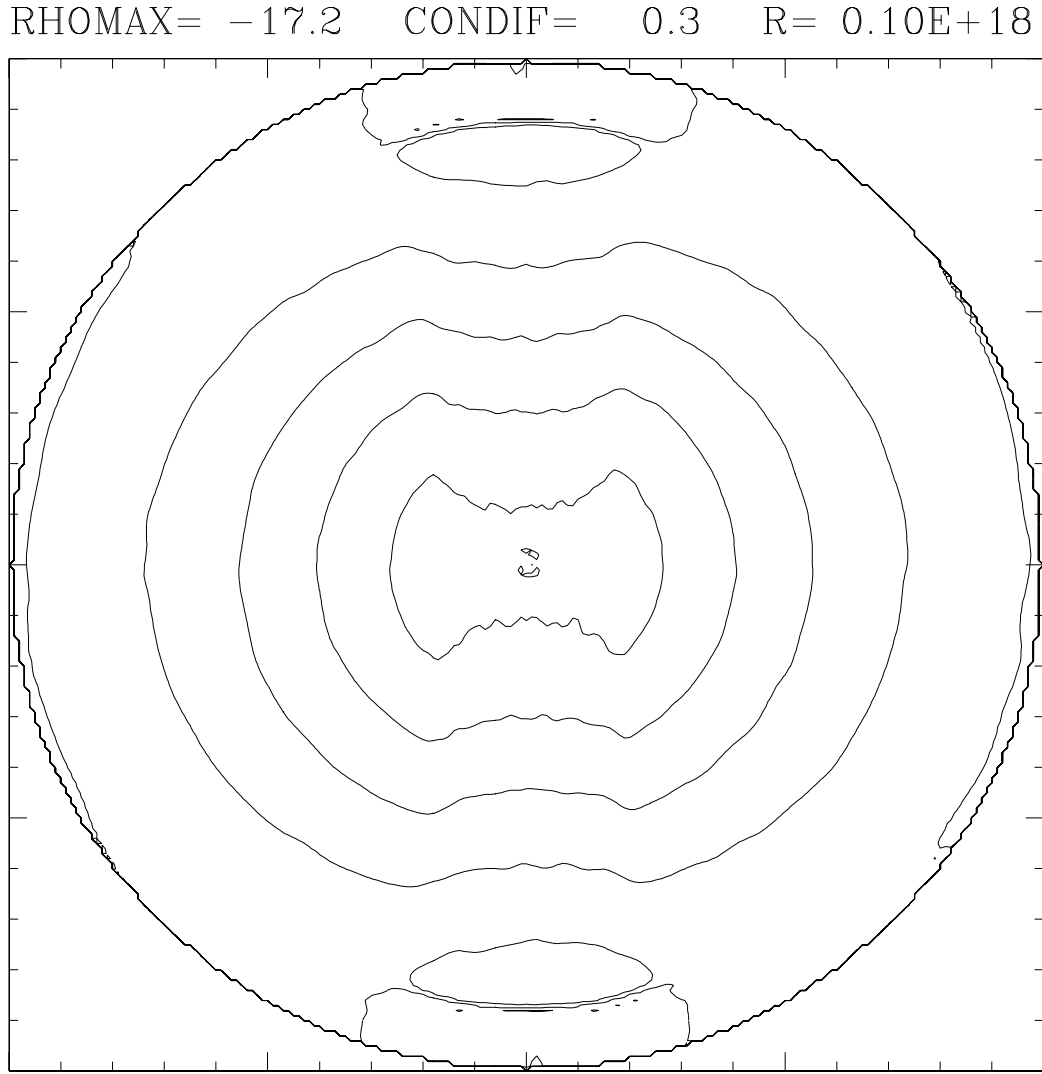


Fig. 3.— Density contours in the equatorial plane for model mbf2g after $1.858 t_{ff}$, plotted as in Figure 1.

RHOMAX= -16.9 CONDIF= 0.3 R= 0.10E+18

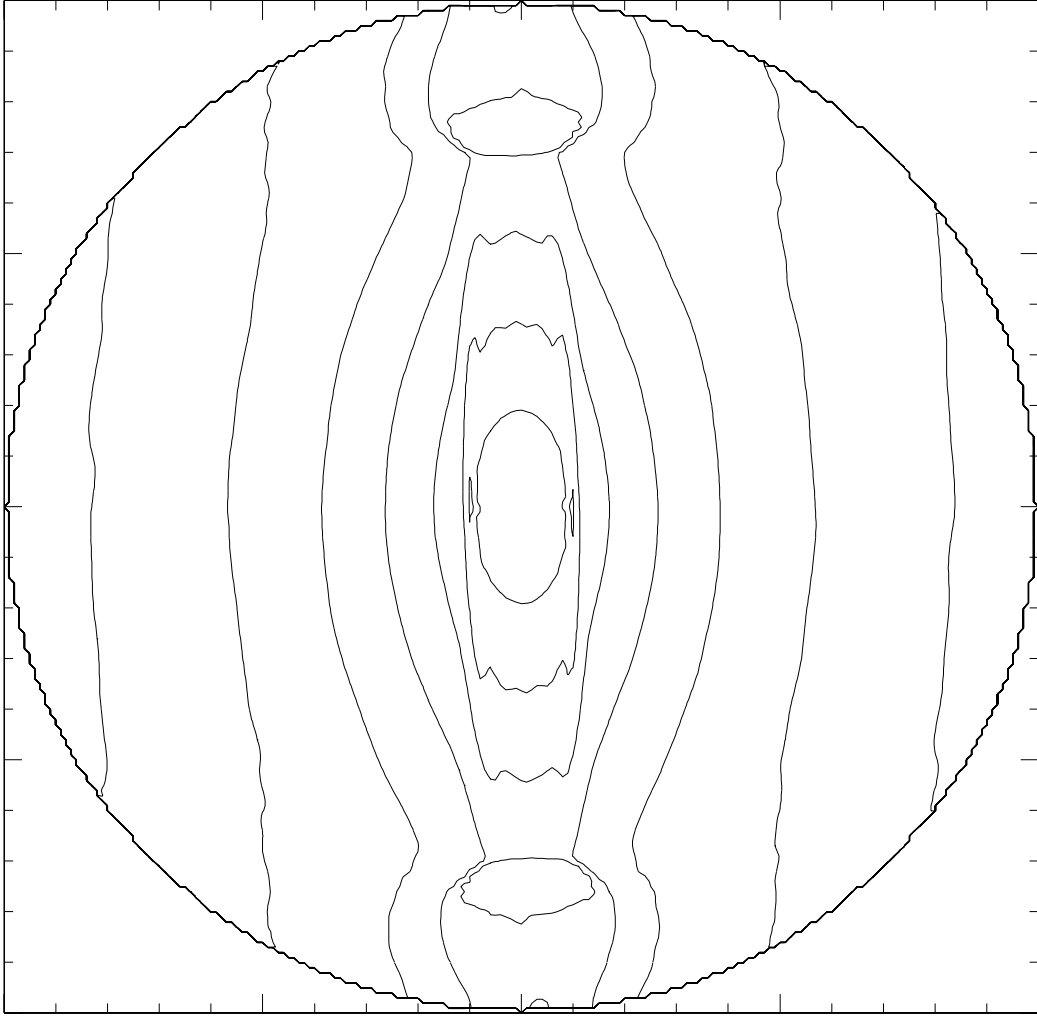


Fig. 4.— Same as Figure 3, but after $2.790 t_{ff}$.

RHOMAX= -16.9 CONDIF= 0.3 R= 0.10E+18

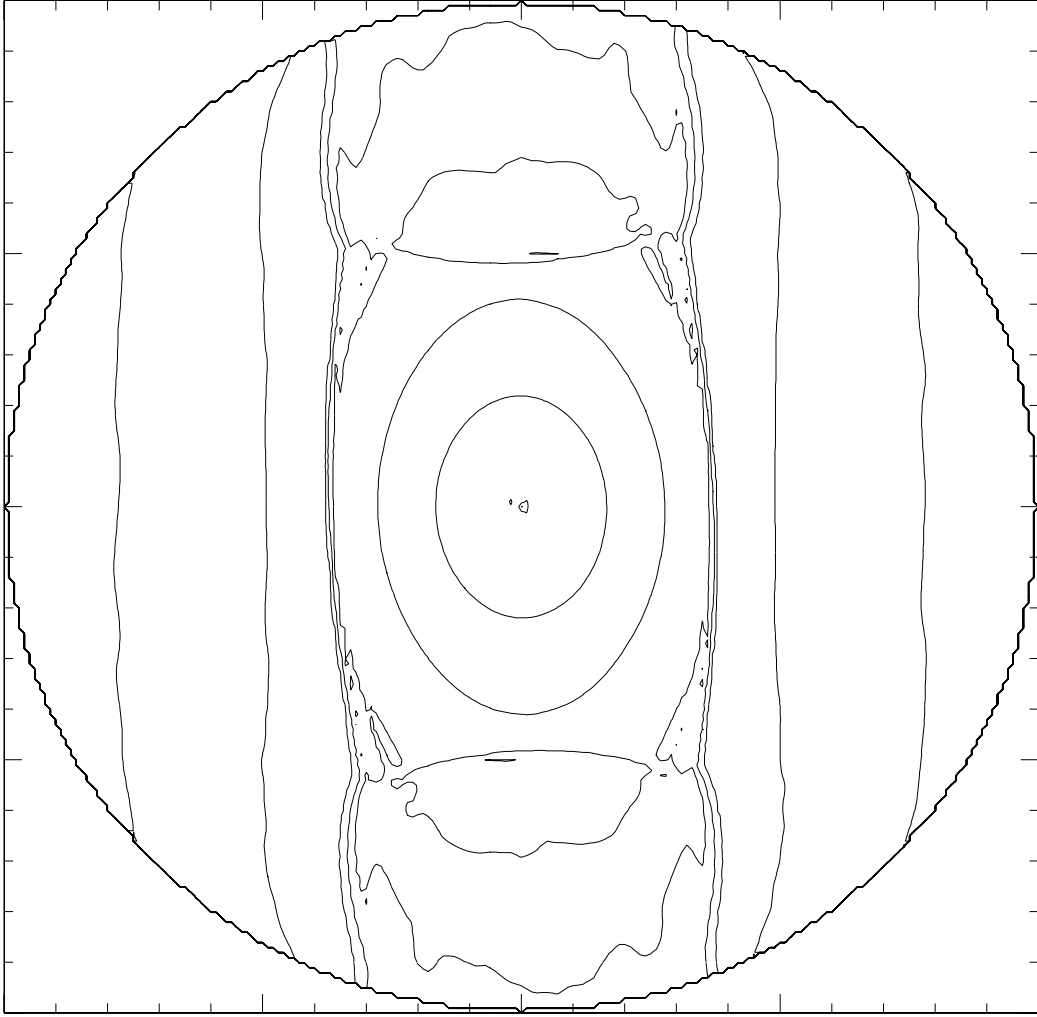


Fig. 5.— Same as Figure 3, but after $3.758 t_{ff}$.

RHOMAX= -16.9 CONDIF= 0.3 R= 0.10E+18

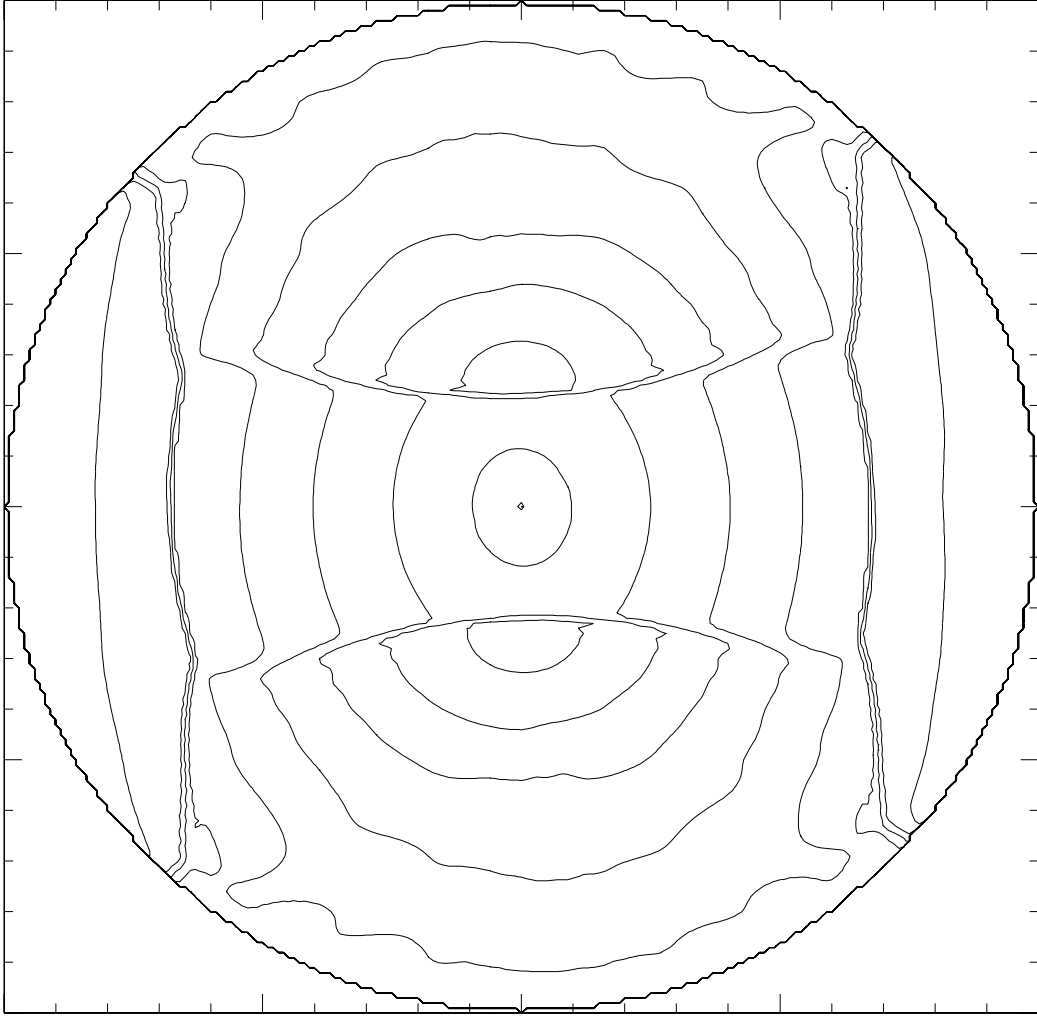


Fig. 6.— Same as Figure 3, but after $4.666 t_{ff}$.

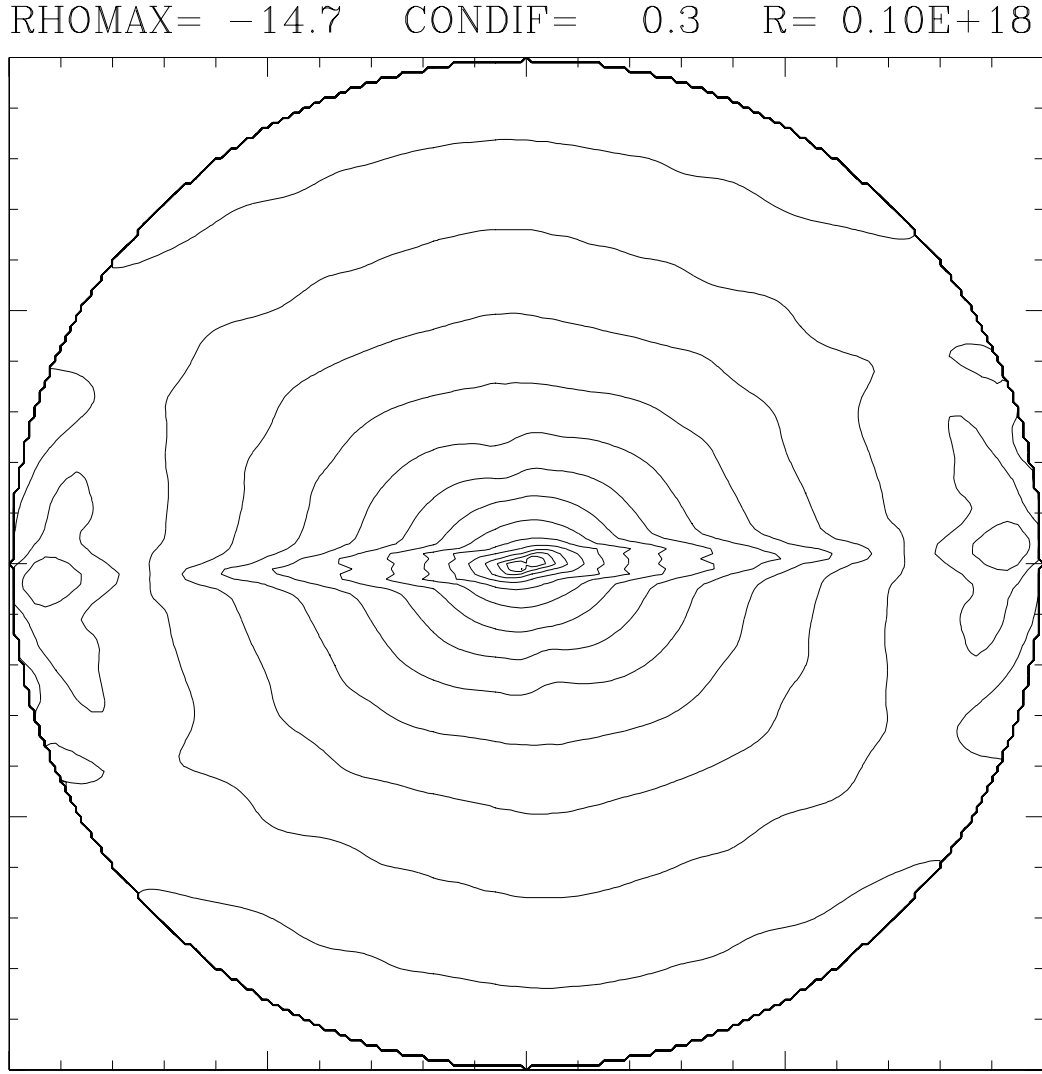


Fig. 7.— Same as Figure 3, but after $5.632 t_{ff}$.

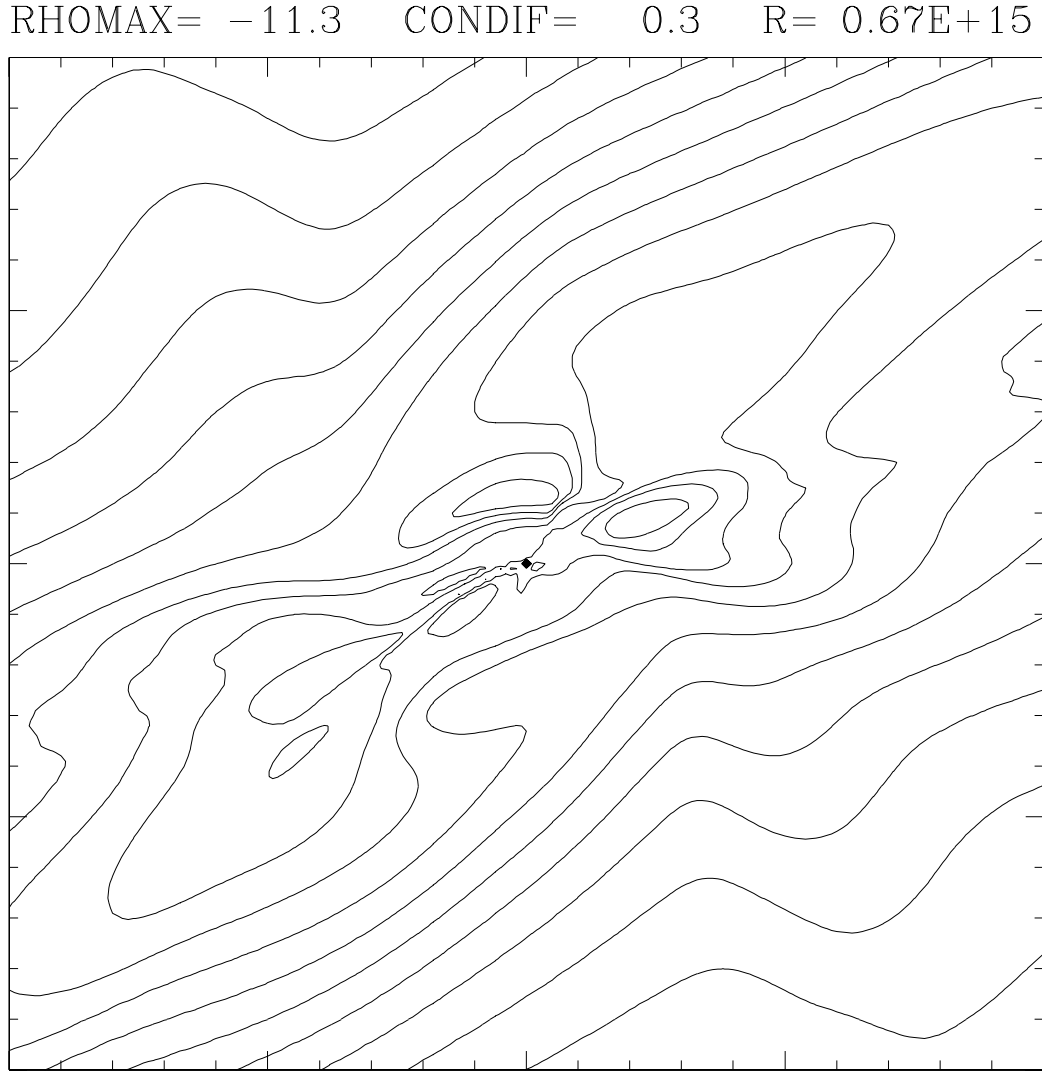


Fig. 8.— Same as Figure 3, but after $5.699 t_{ff}$. Radius of region shown is 6.7×10^{14} cm.

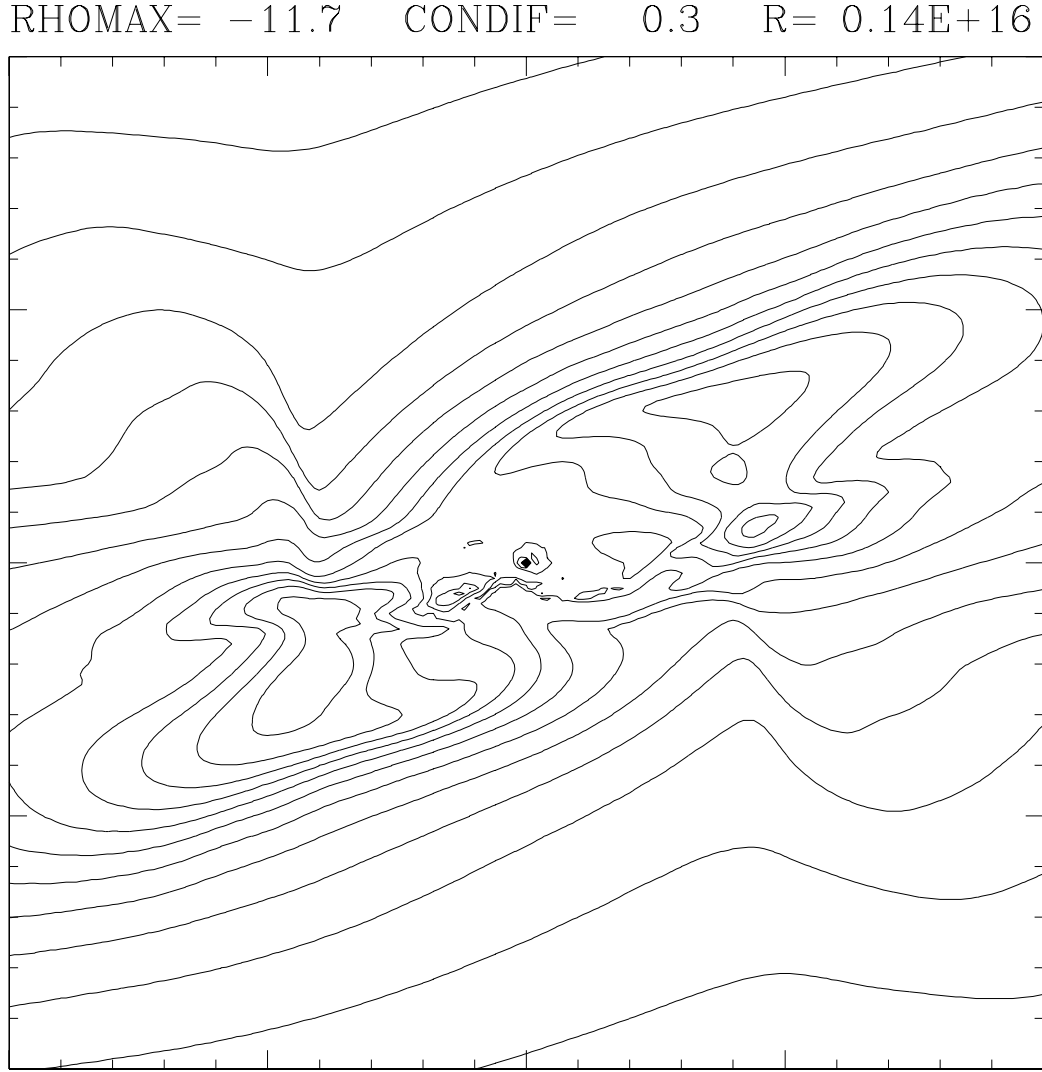


Fig. 9.— Density contours in the equatorial plane for model mbf2e after $5.707 t_{ff}$. Radius of region shown is 1.4×10^{15} cm.

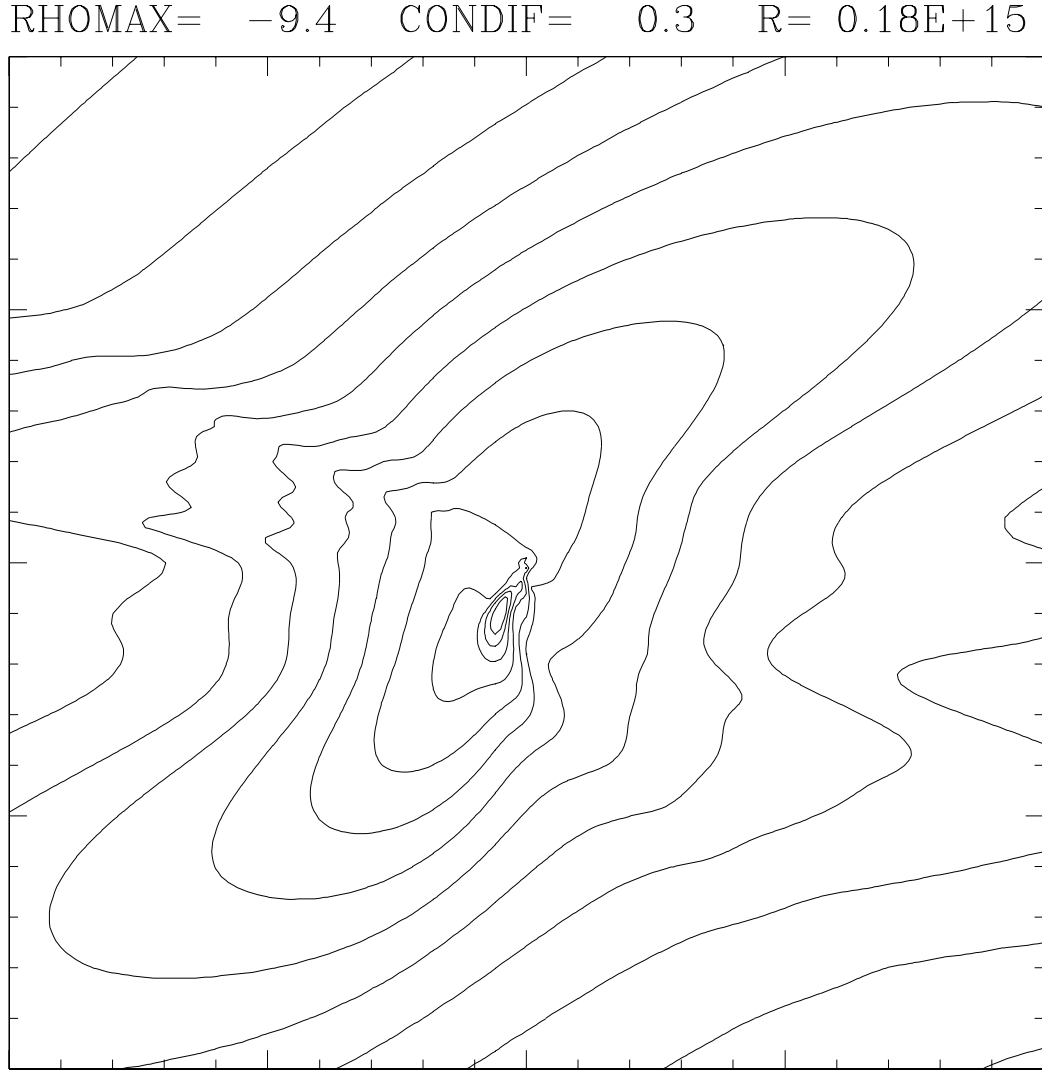


Fig. 10.— Density contours in the equatorial plane for model mbf2f after $6.056 t_{ff}$. Radius of region shown is 1.8×10^{14} cm.

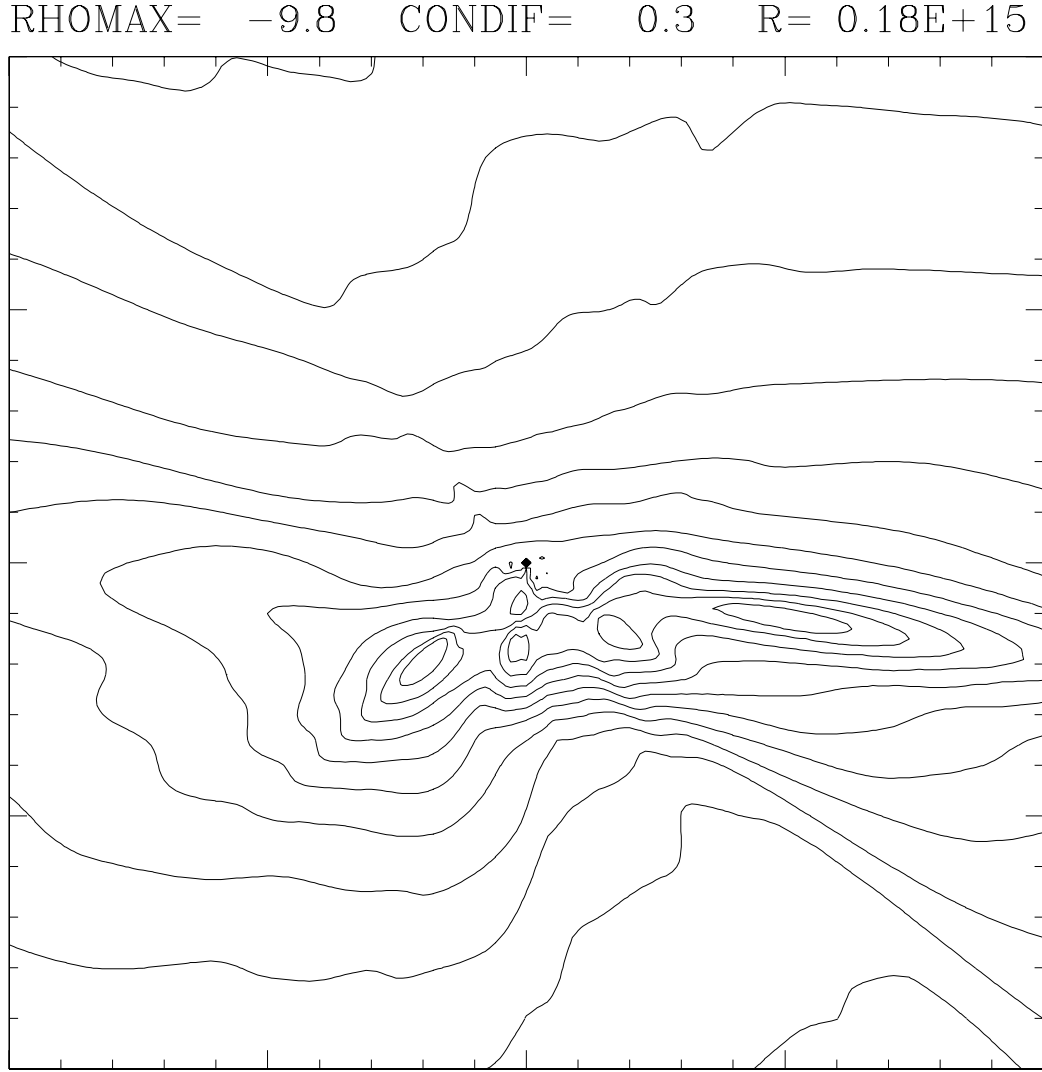


Fig. 11.— Density contours in the equatorial plane for model mbfn after $12.091 t_{ff}$. Radius of region shown is 1.8×10^{14} cm.